Inorganic Chemistry
Article
pubs.acs.org/IC

Tunable Color of $Ce^{3+}/Tb^{3+}/Mn^{2+}$-Coactivated $CaScAlSiO_6$ via Energy Transfer: A Single-Component Red/White-Emitting Phosphor

Wei Lü,[†] Ning Guo,[†,‡] Yongchao Jia,[†,‡] Qi Zhao,[†,‡] Wenzhen Lv,[†,‡] Mengmeng Jiao,[†,‡] Baiqi Shao,[†,‡] and Hongpeng You*[,†]

[†]State Key Laboratory of Rare Earth Resource Utilization, Changchun Institute of Applied Chemistry, Chinese Academy of Sciences, Changchun 130022, People's Republic of China

[‡]Graduate University of the Chinese Academy of Sciences, Beijing 100049, People's Republic of China

ABSTRACT: A series of single-component red/white-emitting $CaScAlSiO_6:Ce^{3+},Tb^{3+},Mn^{2+}$ phosphors have been synthesized by a solid-state reaction. It is observed that $CaScAlSiO_6:Ce^{3+},Tb^{3+}$ phosphors exhibit two dominating bands situated at 380 and 542 nm, originating from the allowed 5d → 4f transition of the Ce^{3+} ion and the $^5D_4 \rightarrow {}^7F_J$ = (J = 6, 5, 4, 3) transition of the Tb^{3+} ion, respectively. As for $CaScAlSiO_6:Ce^{3+},Mn^{2+}$, our results indicate that Mn^{2+} may occupy not only a Ca^{2+} site to generate an orange emission [Mn^{2+}(I)] at 590 nm but also a Sc^{3+} site to generate a red emission [Mn^{2+}(II)] at 670 nm. Both energy transfers from Ce^{3+} to Tb^{3+} and from Ce^{3+} to Mn^{2+} in the $CaScAlSiO_6$ host are investigated and have been demonstrated to be of the resonant type via a dipole−dipole mechanism. By proper tuning of the relative composition of Tb^{3+}/Mn^{2+}, white light can also be achieved upon excitation of UV light, indicating that the developed phosphor may potentially be used as a single-component red/white-emitting phosphor for UV-light-emitting diodes.

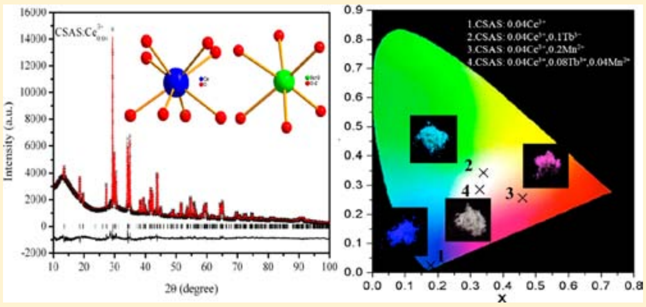

1. INTRODUCTION

Phosphor-converted white-light-emitting diodes (LEDs) have gained enormous commercial interest because of their high luminous efficiency, long lifetimes, environmentally friendly features, etc.[1−4] The most dominant way to create a white LED is by combining a blue InGaN chip with $Y_3Al_5O_{12}:Ce^{3+}$(YAG:Ce)-based yellow phosphors.[5,6] However, the device based on this phosphor exhibits a poor color-rendering index and a high correlated color temperature because of the lack of red light at long wavelength and limits expansion of the LED application.[7−9] Current lighting technology employs UV LED chips with red, green, and blue phosphors to improve this problem. This approach provides white LEDs with excellent color-rendering indexes and can generate warm white light, but the luminescence efficiency is low in this system owing to the strong reabsorption of blue light by the red and green phosphors.[10−12] Recently, many researchers have exploited and fabricated novel multicolor-emitting phosphors into a UV/NUV chip, but disadvantages of poor luminous efficiency resulting from energy reabsorption in these cases also existed.[13−16] In this regard, the search for a new single-component phosphor pumped by UV chips is of significance for white LEDs to avoid the intrinsic color balance, device complication, and high-cost problems associated with using multicolor-emitting components.

In view of the luminescent species, the Ce^{3+} ion not only exhibits good performances for its special optical properties of broad band emission but also can act as an efficient sensitizer. Recently, many researchers have studied the energy-transfer mechanism between Ce^{3+} and Tb^{3+} or Ce^{3+} and Mn^{2+} in a proper single host lattice for LED application, such as $Na_2Gd_2B_2O_7:Ce^{3+},Tb^{3+}$,[17] $Ca_2Al_3O_6F:Ce^{3+},Tb^{3+}$,[18] $Ca_3Sc_2Si_3O_{12}:Ce^{3+},Mn^{2+}$,[19,20] and YAG:$Ce^{3+},Mn^{2+},Si^{4+}$.[21] In these systems, the luminescent efficiency of Tb^{3+} and Mn^{2+} singly doped phosphors is very low upon UV/blue-light excitation because of the 4f−4f weak absorption for Tb^{3+} and the forbidden $^4T_1 \rightarrow {}^6A_1$ transition for Mn^{2+}.[22,23] However, by the introduction of an efficient sensitizer of Ce^{3+}, the energy would be transferred from the 5D level of Ce^{3+} to the $^5D_{3,4}$ level of Tb^{3+} or to the 4G level of Mn^{2+}, which helps Tb^{3+} and Mn^{2+} ions to emit efficiently. In particular, when Tb^{3+} and Mn^{2+} were both doped into the same host matrix, their emission colors can be easily tuned by varying the relative compositions of Tb^{3+}/Mn^{2+}. This advantage has been utilized to develop new tridoped phosphors, which were reported by many research groups.[24−28]

In this research, we report our recent investigation results on the luminescence and color tunability of a red/white-emitting $CaScAlSiO_6:Ce^{3+},Tb^{3+},Mn^{2+}$ phosphor. To the best of our knowledge, there has been no reported study on $Ce^{3+}/Tb^{3+}/Mn^{2+}$ activated or coactivated in the $CaScAlSiO_6$ host in the literature. By variation of the relative dopant concentrations of Tb^{3+} and Mn^{2+}, red/white light can be generated with higher

Received: November 11, 2012
Published: February 27, 2013

color stability. Energy transfers from Ce^{3+} to Tb^{3+} and from Ce^{3+} to Mn^{2+} are investigated according to the Inokuti–Hirayama theoretical model.

2. EXPERIMENTAL SECTION

2.1. Sample Preparation. The $Ca_{1-x-z}Sc_{1-y}AlSiO_6$(CSAS):-$x$$Ce^{3+}$,$y$$Tb^{3+}$,$z$$Mn^{2+}$ phosphors were synthesized by a high-temperature solid-state reaction. The constituent oxides or carbonates $CaCO_3$ (99.9%), Sc_2O_3 (99.9%), SiO_2 (99.9%), Al_2O_3 (99.9%), CeO_2 (99.99%), Tb_4O_7 (99.99%), and $MnCO_3$ (99.99%) were employed as raw materials, which were mixed homogeneously by an agate mortar for 30 min, placed in a crucible with a lid, and then sintered in a tubular furnace at 1400 °C for 4 h in a reductive atmosphere (10% H_2 + 90% N_2 mixed flowing gas).

2.2. Measurements and Characterization. The structure of sintered samples was identified by powder X-ray diffraction (XRD) analysis (Bruker AXS D8), with graphite-monochromatized Cu Kα radiation (λ = 0.15405 nm) operating at 40 kV and 40 mA. Crystal structure refinement employed the Rietveld method, as implemented in the *General Structure Analysis System* (*GSAS*) program.[29] The measurements of photoluminescence (PL) and photoluminescence excitation (PLE) spectra were performed using a Hitachi F4500 spectrometer equipped with a 150 W xenon lamp under a working voltage of 700 V. The excitation and emission slits were both set at 2.5 nm. The luminescence decay curve was obtained from a Lecroy Wave Runner 6100 digital oscilloscope (1 GHz) using a tunable laser (pulse width = 4 ns; gate = 50 ns) as the excitation source (Continuum Sunlite OPO). The quantum efficiency yields were analyzed with a PL quantum-efficiency measurement system (C9920-02, Hamamatsu Photonics, Shizuoka, Japan) by a 150 W xenon lamp. All of the measurements were performed at room temperature.

3. RESULTS AND DISCUSSION

3.1. XRD Refinement. The experimental (crosses), calculated (solid line), and difference (bottom) XRD profiles for the Rietveld refinement of CSAS:0.02Ce^{3+} are shown in Figure 1. The starting structural model was constructed with crystallographic data previously reported for CSAS (JCPDS 77-0465).[30] All of the observed XRD peaks are obtained with goodness-of-fit parameters R_{wp} = 6.11% and χ^2 = 4.293. CSAS has space group $C2/c$ with unit cell parameters a = 9.877 Å, b = 9.003 Å, and c = 5.446 Å. The crystallographic data and selected bond lengths are summarized in Table 1. The average bond distances for Ca–O and Sc–O for the CSAS compounds in the present work are 2.5142 and 2.1028 Å, respectively. These values are similar to the typical values of the Ca–O and Sc–O bonds [Ca–O = 2.390(4) Å and Sc–O = 2.099(6) Å] in the $Ca_3Sc_2Si_3O_{12}$ system. Figure 1, inset, shows the coordination environments of CASC compounds, in which two types of independent cation sites are found, namely, an 8-fold-coordinated Ca^{2+} site and a 6-fold-coordinated Sc^{2+} site. On the basis of the effective ionic radii (r) of cations with different coordination numbers (CNs) as reported by Shannon,[31] it is demonstrated that Ce^{3+} is expected to occupy a Ca^{2+} site because the ionic radius of Ce^{3+} (1.14 Å) is close to that of Ca^{2+} (1.12 Å). As for Tb^{3+} (0.92 Å for CN = 6, 1.04 Å for CN = 8), it is uncertain where the Tb^{3+} ions exactly occupy. However, accounting for ion valence, we presume that Tb^{3+} may be favorable to occupying Sc^{3+}. When Mn^{2+} is incorporated into the crystal structure of CSAS, we propose that Mn^{2+} may substitute both Ca^{2+} and Sc^{3+} sites, because the Mn^{2+} ionic radius (r = 0.96 Å for CN = 8; r = 0.83 Å for CN = 6) is not only close to that of Ca^{2+} (r = 1.12 Å for CN = 8) but also similar to that of Sc^{3+} (r = 0.75 Å for CN = 6). Mn^{2+} substitution for Ca^{2+} and Sc^{3+} is actually observed in the PL spectra of the samples presented in section 3.3.

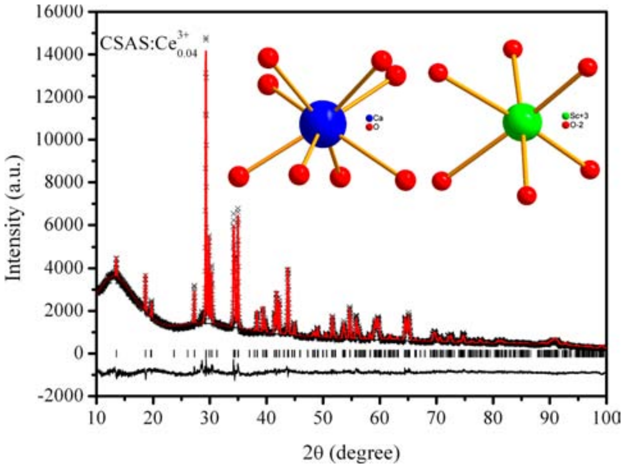

Figure 1. Experimental (crosses), calculated (solid line), and difference (bottom) XRD profiles for the Rietveld refinement of CSAS:0.02Ce^{3+}. The rather unusual background in the 10–20° range is an artifact going back to the setup of the evacuated flat sample holder.

Table 1. Crystallographic Data and Selected Bond Lengths

crystallographic data of CSAS		seleted bond lengths (Å)	
radiation type/Å	1.54056	Ca–O1	2.44955(8)
2θ range/deg	10–100	Ca–O2	2.38465(10)
T/K	295	Ca–O3	2.54429(8)
symmetry	monoclinic	Ca–O3	2.67847(8)
space group	$C2/c$	Sc–O1	2.18422(7)
a/Å	9.877	Sc–O1	2.10339(9)
b/Å	9.003	Sc–O2	2.02073(6)
c/Å	5.446	Si–O1	1.68834(9)
α/deg	90	Si–O2	1.66463(6)
β/deg	106	Si–O3	1.70776(5)
γ/deg	90	Si–O3	1.72112(6)
volume/Å	465.91	Al–O1	1.68834(3)
R_p/%	4.51	Al–O2	1.66463(6)
R_{wp}/%	6.11	Al–O3	1.70776(5)
χ^2	4.293	Al–O3	1.72112(6)

3.2. Luminescence Properties and Energy Transfer in CSAS:Ce^{3+},Tb^{3+}. Figure 2 shows the PL and PLE spectra in CSAS:0.02Ce^{3+} (a), CSAS:0.1Tb^{3+} (b) and CSS:0.02Ce^{3+},0.1Tb^{3+} (c). It can be seen that the excitation spectrum of CSAS:Ce^{3+} (monitored at 380 nm) consists of three components, having peaks at 245, 296, and 340 nm (the strongest), respectively, which correspond to the electronic transitions from the ground state to the different crystal-field-splitting bands of excited 5d states of Ce^{3+}, while the emission spectrum appears as an intense violet light with a peak at 380 nm, which originated from the 5d → 4f transition of Ce^{3+}. The PLE spectrum of Tb^{3+} consists of several lines in the region from 300 to 500 nm, which correspond to the absorption f–f transition of the Tb^{3+} ion. The Tb^{3+} emission lines are located at 485, 542, 580, and 620 nm, which are assigned to the $^5D_4 \rightarrow {}^7F_J$ = (J = 6, 5, 4, 3) multiplet transitions, respectively. Compared to the PL spectrum of CSAS:Ce^{3+} (Figure 2a), that of CSAS:Tb^{3+} shows very weak emission upon UV-light excitation due to forbidden f–f absorption transitions of Tb^{3+}

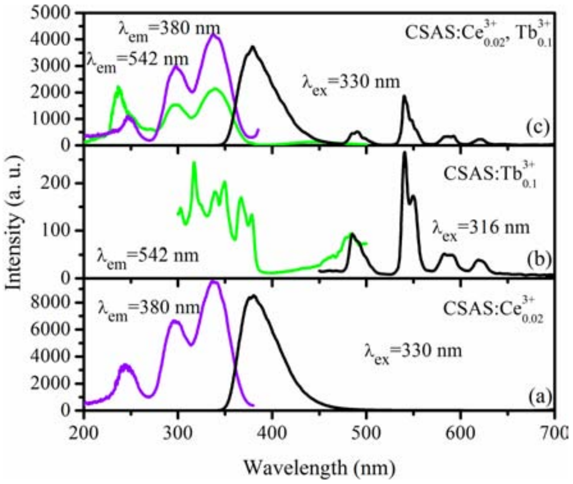

Figure 2. PL and PLE spectra in CSAS:0.02Ce^{3+} (a), CSAS:0.1Tb^{3+} (b), and CSS:0.02Ce^{3+},0.1Tb^{3+} (c).

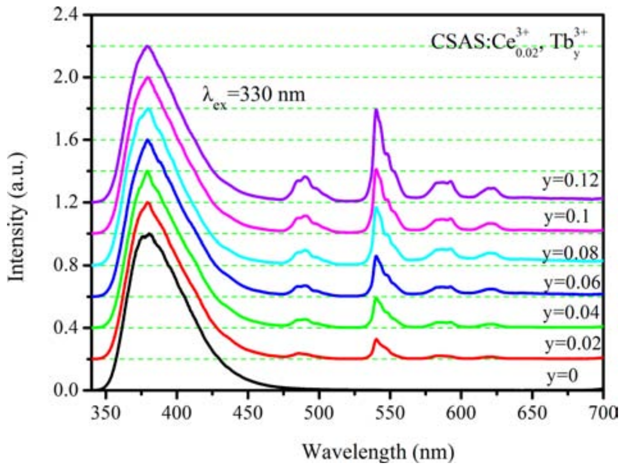

Figure 3. Series of emission spectra for CSAS:0.02 Ce^{3+},yTb^{3+} (y = 0, 0.02, 0.04, 0.06, 0.08, 0.10, 0.12) under UV excitation (λ_{ex} = 330 nm).

in UV. It is clearly exhibited that there is a significant spectral overlap between the Ce^{3+} PL and Tb^{3+} PLE spectra, indicating the possibility of energy transfer from Ce^{3+} to Tb^{3+} in CSAS. Figure 2c illustrates the PLE and PL spectra of CSAS:0.02-Ce^{3+},0.1Tb^{3+}. It is observed that the PLE spectrum monitoring the 542 nm emission of Tb^{3+} is similar to that monitoring the violet emission of Ce^{3+}, demonstrating the existence of energy transfer from Ce^{3+} to Tb^{3+}, while the emission intensity of Tb^{3+} is considerably enhanced compared to the Ce^{3+} emission because of energy transfer from Ce^{3+} to Tb^{3+}. Figure 3 shows a series of emission spectra for CSAS:0.02Ce^{3+},yTb^{3+} (y = 0, 0.02, 0.04, 0.06, 0.08, 0.10, 0.12) under UV excitation (λ_{ex} = 330 nm). With increasing Tb^{3+} concentration, the emission intensities of Tb^{3+} increase followed by decreases of the Ce^{3+} emission intensities, reflecting the result of energy transfer from Ce^{3+} to Tb^{3+}.

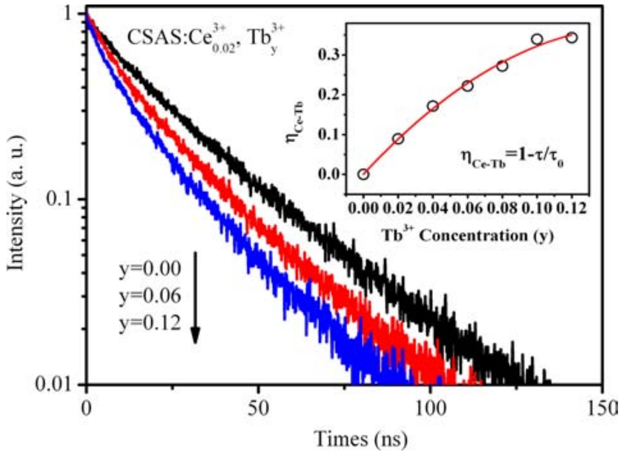

Figure 4. Fluorescence lifetimes τ for Ce^{3+} with different Tb^{3+} concentrations. Inset: Calculated energy-transfer efficiency with different doping Tb^{3+} contents.

To further validate the process of energy transfer, the fluorescence lifetimes τ for Ce^{3+} with different Tb^{3+} concentrations are measured and presented in Figure 4. The values of the lifetimes are obtained by integrating the decay curves, of which the initial intensities are normalized. With increasing Tb^{3+} concentration, the fluorescence decreases and tends to be a nonexponential function with increasing Tb^{3+} concentrations, reflecting the characteristics of energy transfer between Ce^{3+} and Tb^{3+}.[32] The energy-transfer efficiency η_{Ce-Tb} can be calculated using

$$\eta_{Ce-Tb} = 1 - \tau/\tau_0 \qquad (1)$$

where τ_0 is the lifetimes for Ce^{3+} in the absence of Tb^{3+}. The calculated energy-transfer efficiency is shown in Figure 4, inset. The efficiency η_{Ce-Tb} increases with increasing x and reaches 35% at y = 0.12.

The decays in Figure 4 change from exponential to nonexponential patterns with increasing x, reflecting the effect of energy transfer. If the donor and acceptor ions are uniformly distributed in the host, the migration process is negligible compared to energy transfer between donors and acceptors. The normalized intensity of the donor fluorescence can be written as

$$I_D(t) = I_{D0}(t)\,f(t) \qquad (2)$$

where $I_{D0}(t)$ is the decay function of donors in the absence of acceptors and the function $f(t)$ characterizes the loss of excited donors due to one-way energy transfer to the acceptors. According to the Inokuti–Hirayama formula,[32] we have

$$f(t) = \exp\left[-\frac{4}{3}\pi\Gamma\left(1 - \frac{3}{m}\right)n_A\alpha^{3/m}t^{3/m}\right] \qquad (3)$$

where α is a rate constant for energy transfer, m = 6, 8, and 10 are the coefficients for dipole–dipole, dipole–quadrupole, and quadrupole–quadrupole interactions, respectively, and n_A is the number of acceptor ions per unit volume. From eqs 2 and 3, $\log\{\ln[I_{D0}(t)/I_D(t)]\}$ acts as a linear function of $\log(t)$ with a slope of $3/m$. In order to well understand the Ce–Tb energy-transfer process, we plot $\log\{\ln[I_{D0}(t)/I_D(t)]\}$ versus $\log(t)$ for various samples, as shown in Figure 5. The values of S estimated from the slope were found to be 5.87, 5.94, and 6.05 for CSAS:0.02Ce^{3+},yTb^{3+} samples with n = 0.04, 0.06, and 0.08, respectively. The values are nearly coincident with the conventional value of m = 6, indicating that the dominant interaction mechanism for CSAS:Ce^{3+},Tb^{3+} is based on the dipole–dipole interaction.

For the dipole–dipole interaction mechanism, the critical distance (R_c) for energy transfer from Ce^{3+} to Tb^{3+} can be obtained by the spectral overlap method:[33]

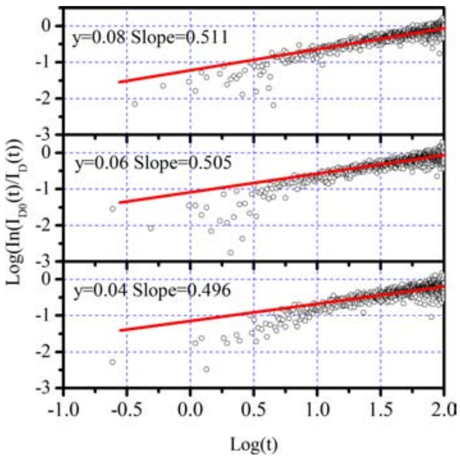

Figure 5. $\log\{\ln[I_{D0}(t)/I_D(t)]\}$ vs $\log(t)$ for various Tb^{3+} contents.

$$R_c^{6} = 3.024 \times 10^{12} f_q \int \frac{F_S(E)\,F_A(E)\,dE}{E^4} \tag{4}$$

where f_q is the oscillator strength of the involved absorption transition of the acceptor (Tb^{3+}),[34] λ_S (in Å) is the wavelength position of the sensitizer's emission, E is the energy involved in the transfer (in eV), and $\int F_S(E)\,F_A(E)\,dE/E^4$ represents the spectral overlap between the normalized shapes of the Ce^{3+} emission $F_S(E)$ and the Tb^{3+} excitation $F_A(E)$, and in our case, it is calculated to be about 0.0114 eV^{-5}. Using the above equation with $f_q = 10^{-6}$, the critical distance R_c was estimated to be 5.8 Å.

3.3. Luminescence Properties and Energy Transfer in CSAS:Ce^{3+},Mn^{2+}.

The PL and PLE spectra of the Ce^{3+} and Mn^{2+} singly doped CSAS phosphors are shown in Figure 6a,b.

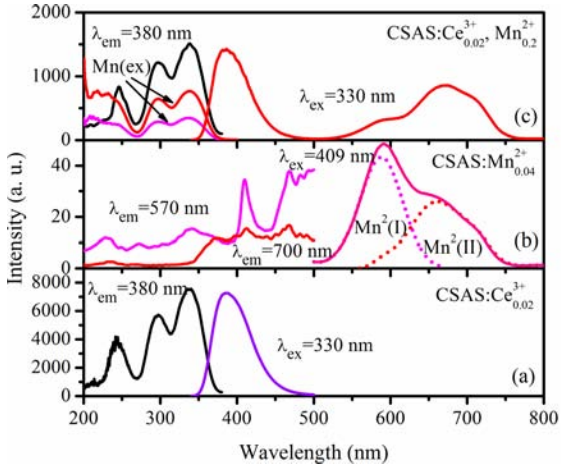

Figure 6. PL and PLE spectra in CSAS:0.02Ce^{3+} (a), CSAS:0.04Mn^{2+} (b), and CSS:0.02Ce^{3+},0.2Mn^{2+} (c).

The PL spectrum of Mn^{2+} singly doped CSAS exhibits two emission bands: one is a yellow emission band around 590 nm [named Mn^{2+}(I)], and the other one is a red emission band around 670 nm [named Mn^{2+}(II)]. The shape of the PLE spectrum monitored at 590 nm is remarkably different from that monitored at 670 nm. Therefore, we infer that there exist two types of Mn^{2+} luminescent centers in the CSAS system. As we know, the crystal structure of CSAS provides two different sites for the cautions in it, i.e., a 8-fold-coordinated Ca^{2+} site and a 6-fold-coordinated Sc^{2+} site. Thus, the observed two emission bands of Mn^{2+} [Mn^{2+}(I) and Mn^{2+}(II)] indicate that Mn^{2+} ions can occupy both Ca^{2+} and Sc^{3+} sites. Considering that the average distance for Ca−O (2.5142 Å) is significantly longer than that for Sc−O (2.1028 Å),[31] it is therefore speculated that the crystal-field effects for the Ca^{2+} site are weaker than those for the Sc^{3+} site. For this reason, we believe that the band at 590 nm is assigned to Mn^{2+}(I) occupying Ca^{2+} with a weak crystal field and the other one at 670 nm corresponds to Mn^{2+}(II) occupying Sc^{3+} with a strong crystal field. Similar observations were also reported by Liu et al. for Ce^{3+}-doped $Ca_3Sc_2Si_3O_{12}$.[19] Figure 6c illustrates the PLE and PL spectra of CSAS:0.02Ce^{2+},0.2Mn^{2+}. It is found that the PLE spectra monitoring the yellow emission of Mn^{2+}(I) and the red emission of Mn^{2+}(II) are all similar to those monitoring the blue emission of Ce^{3+}, demonstrating the existence of energy transfer from Ce^{3+} to Mn^{2+} in CASC systems. Meanwhile, the Mn^{2+} emission intensities are enhanced greatly compared to Mn^{2+} singly doped CASC. These results give strong evidence of the effective Ce^{3+}−Mn^{2+} energy transfer. The occurrence of energy transfer can be clearly understood as noticing the spectral overlap between the Ce^{3+} emission band in CSAS:0.02Ce^{3+} and the Mn^{2+} excitation band in CSAS:0.04Mn^{2+}. Figure 7 shows the normalized emission spectra for CSAS:0.02Ce^{3+},$z$$Mn^{2+}$ phosphors with increasing z from 0 to 0.20, which were measured at an excitation wavelength of 330 nm. With increasing concentration of Mn^{2+}, the emission intensity of Mn^{2+} ions increases systematically due to Ce^{3+}−Mn^{2+} energy transfer. In addition, it is noticeable that the relative emission intensity of the Mn^{2+}(I) ions decreases, which might be due to concentration quenching.

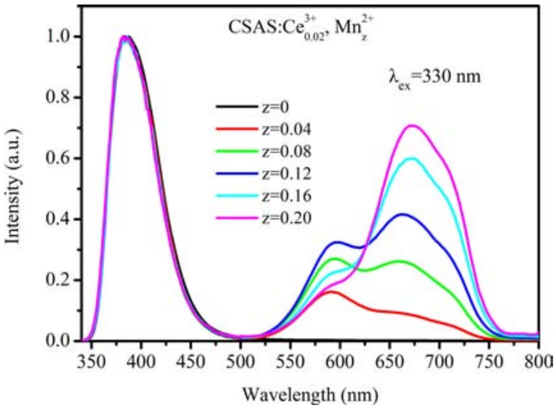

Figure 7. Normalized emission spectra for CSAS:0.02Ce^{3+},$z$$Mn^{2+}$ phosphors with increasing z from 0 to 0.20 under UV excitation (λ_{ex} = 330 nm).

The decay curves of Ce^{3+} fluorescence in CSAS:0.02Ce^{3+},$z$$Mn^{2+}$ (z = 0, 0.04, 0.08, 0.12, 0.16, and 0.2) are also measured and shown in Figure 8. The reduction of the lifetimes for Ce^{3+} with increasing Mn^{2+} concentrations is observed. These results support the efficient energy transfer from Ce^{3+} to Mn^{2+}. The energy-transfer efficiency can be obtained using eq 1, as shown in Figure 8, inset. It can be seen that the values of the energy-transfer efficiency η_{Ce-Mn} gradually increase and reach 54% for Mn^{2+} concentrations at z = 0.2, further implying that the energy of the red emission of Mn^{2+} is derived from Ce^{3+}. Using eqs 2 and 3, the value of S was also estimated from the slope and found to be 6.11, 5.91, and 6.14 for

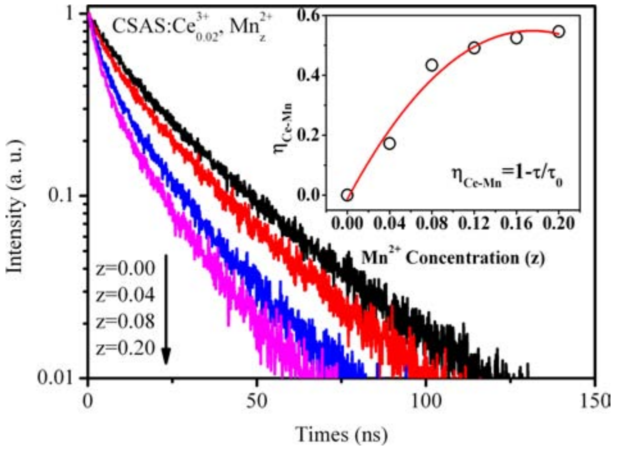

Figure 8. Decay curves of Ce^{3+} fluorescence in CSAS:$0.02Ce^{3+}$,zMn^{2+} (z = 0, 0.04, 0.08, 0.12, 0.16, and 0.2) Inset: Energy-transfer efficiency (η_{Ce-Mn}) with different doping Mn^{2+} contents.

CSAS:$0.02Ce^{3+}$,zMn^{2+} samples with z = 0.04, 0.08, and 0.12, respectively, as shown in Figure 9. These values are nearly coincident with the conventional value of m = 6, meaning that the nature of multipolar interaction for energy transfer between the donor and acceptor is also mainly governed by dipole–dipole interaction.

3.4. Quantum Yields (QYs) and Chromaticity of CSAS:Ce^{3+},Tb^{3+},Mn^{2+}.

XRD patterns of CSAS:Ce^{3+},Tb^{3+},Mn^{2+} with various Tb^{3+} and Mn^{2+} concentrations are shown in Figure 10. All of the observed peaks can be indexed to the standard data of CSAS with JCPDS 77-0465. No obvious impurity phase was detected when Tb^{3+} and Mn^{2+} were doped into the host lattice.

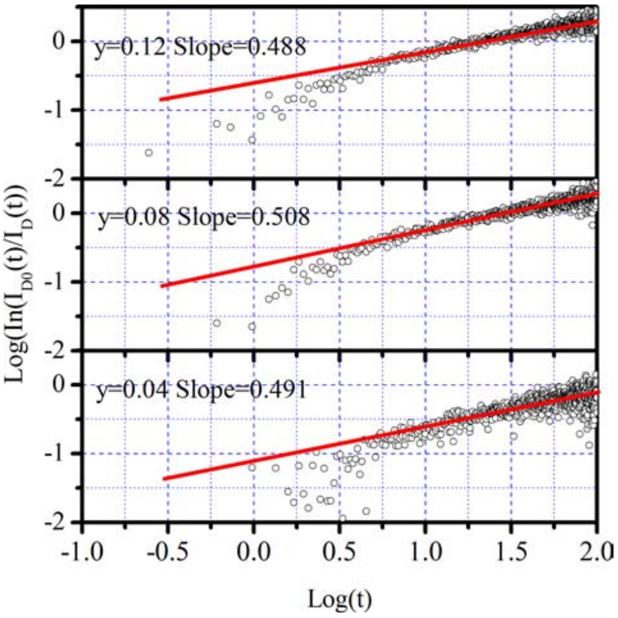

Figure 9. $\log\{\ln[I_{D0}(t)/I_D(t)]\}$ vs $\log(t)$ for various Mn^{2+} contents.

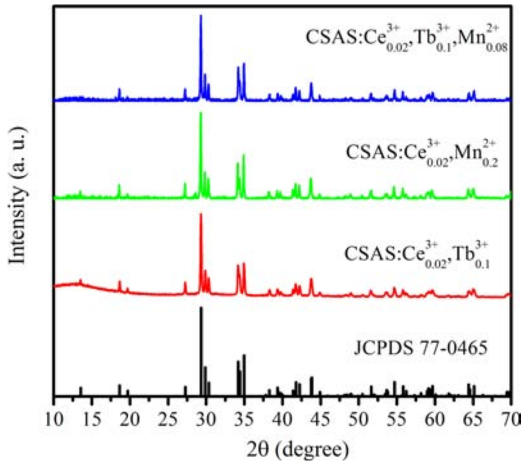

Figure 10. XRD patterns of CSAS:Ce^{3+},Tb^{3+},Mn^{2+} with varying Tb^{3+} and Mn^{2+} concentrations.

The absolute QY is an important parameter to be considered for practical LED application. So, the absolute QYs of the obtained phosphors were also measured. Upon excitation at 340 nm, for CSAS:Ce^{3+},yTb^{3+} (y = 0, 0.02, 0.04, 0.06, 0.08, 0.10, and 0.12) phosphors, the absolute QYs were determined to be 96.8%, 93.3%, 91.6%, 87.1%, 81.1%, 80.5%, and 79.5%, respectively. For the CSAS:$0.02Ce^{3+}$,zMn^{2+} (z = 0, 0.04, 0.08, 0.12, 0.16, and 0.2) series of samples, the absolute QYs were determined to be 97.1%, 87.6%, 80.4%, 73.4%, 67.3%, and 65.5%, respectively. The high QY of these phosphors indicates that CSAS is a quite suitable matrix for rare-earth ion doping. The CIE chromaticity diagrams of the emitting phosphors CSAS:Ce^{3+},yTb^{3+},zMn^{2+} with different compositional concentrations (y and z) are displayed in Figure 11. The color tone can be tuned from blue (0.17 and 0.03) to white (0.33 and 0.34) by adjusting the concentration of Tb^{3+} and from blue (0.17 and 0.03) to red (0.44 and 0.24) by varying the Mn^{2+} content, respectively. The inset in Figure 11 also shows a series of digital photographs of the selected CSAS:Ce^{3+},yTb^{3+},zMn^{2+} phosphors upon 365 nm UV-lamp excitation. In particular, it is found that CSAS:$0.04Ce^{3+}$,$0.08Tb^{3+}$,$0.04Mn^{2+}$ shows white light, suggesting that it can be used as a potential white-emitting candidate for UV LEDs.

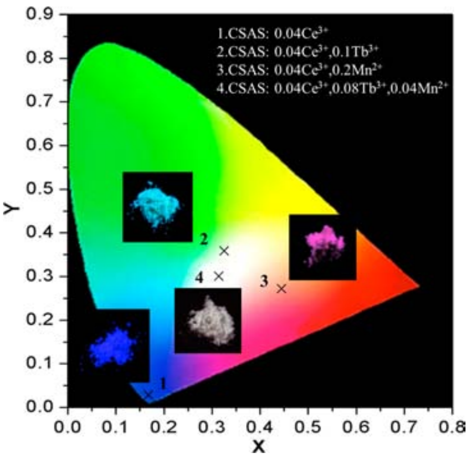

Figure 11. CIE chromaticity diagram and a series of digital photographs of the selected CSAS:Ce^{3+},yTb^{3+},zMn^{2+} phosphors under 365 nm UV-lamp excitation.

4. CONCLUSION

In summary, we have synthesized a series of novel emission-tunable CSAS:Ce^{3+},yTb^{3+},zMn^{2+} phosphors by a solid-state reaction. The obtained phosphor exhibits four emission colors:

a blue band of 380 nm, a green band of 542 nm, a yellow band of 574 nm, and a red band of 670 nm. Mn^{2+} may substitute either for Ca^{2+} to generate a yellow emission band (574 nm) or for Sc^{3+} to generate a red emission band (670 nm). The energy transfer from Ce^{3+} to Tb^{3+} and from Ce^{3+} to Mn^{2+} in a $CaScAlSiO_6$ host matrix was confirmed via a dipole−dipole mechanism by the luminescence spectra and fluorescence decay dynamics based on the Inokuti−Hirayama theoretical model. We have demonstrated that the varied emitted color from blue to green or red and eventually to white can be achieved by proper tuning of the relative ratio of Tb^{3+} and Mn^{2+}. All of these results indicate that CSAS:Ce^{3+},Tb^{3+},Mn^{2+} is a promising single-composition phosphor for application involving white LEDs.

AUTHOR INFORMATION

Corresponding Author

*E-mail: hpyou@ciac.jl.cn.

Notes

The authors declare no competing financial interest.

ACKNOWLEDGMENTS

This work is financially supported by the National Natural Science Foundation of China (Grant No. 21271167), Fund for Creative Research Groups (Grant No. 21221061).

REFERENCES

(1) Feldmann, C.; Jüstel, T.; Ronda, C. R.; Schmidt, P. J. *Adv. Funct. Mater.* **2003**, *13*, 511.

(2) Höppe, H. A. *Angew. Chem., Int. Ed.* **2009**, *48*, 3572.

(3) Xie, R. J.; Hirosaki, N.; Suehiro, T.; Xu, F. F.; Mitomo, M. *Chem. Mater.* **2006**, *18*, 5518.

(4) Tang, Y. S.; Hu, S. F.; Ke, W. C.; Lin, C. C.; Bagkar, N. C.; Liu, R. S. *Appl. Phys. Lett.* **2008**, *93*, 131114.

(5) Nakamura, S.; Fasol, G. *The Blue Laser Diode*; Springer: Berlin, 1996.

(6) Nakamura, S. *MRS Bull.* **2009**, *34*, 101.

(7) Hao, Z. D.; Zhang, J. H.; Zhang, X.; Sun, X. Y.; Luo, Y. S.; Lu, S. Z.; Wang, X. J. *Appl. Phys. Lett.* **2007**, *90* (26), 261113.

(8) Kim, J. S.; Jeon, P. E.; Park, Y. H.; Choi, J. C.; Park, H. L.; Kim, G. C.; Kim, T. W. *Appl. Phys. Lett.* **2004**, *85* (17), 3696.

(9) Yang, W. J.; Chen, T. M. *Appl. Phys. Lett.* **2007**, *90* (17), 171908.

(10) Kido, J.; Shionoya, H.; Nagai, K. *Appl. Phys. Lett.* **1995**, *67*, 2281.

(11) Piao, X. Q.; Horikawa, T.; Hanzawa, H.; Machida, K. *Appl. Phys. Lett.* **2006**, *88*, 161908.

(12) Lee, S. H.; Park, J. H.; Son, S. M.; Kim, J. S.; Park, H. L. *Appl. Phys. Lett.* **2006**, *89*, 221916.

(13) Lee, G.; Han, J. Y.; Im, W. B.; Cheong, S. H.; Young, D. *Inorg. Chem.* **2012**, *51*, 10688.

(14) Huang, C. H.; Chen, T. M. *Inorg. Chem.* **2011**, *50*, 5725.

(15) Han, J. Y.; Im, W. B.; Lee, G.; Jeon, D. Y. *J. Mater. Chem.* **2012**, *22*, 8793.

(16) Huang, C. H.; Wang, D. Y.; Chiu, Y. C.; Yeh, Y. T.; Chen, T. M. *RSC Adv.* **2012**, *2*, 9130.

(17) Guo, C. F.; Jing, H.; Li, T. *RSC Adv.* **2012**, *2*, 2119.

(18) Xia, Z. G.; Liu, R. S. *J. Phys. Chem. C* **2012**, *116* (29), 15604.

(19) Liu, Y. F.; Zhang, X.; Hao, Z. D.; Luo, Y. S.; Wang, X. J.; Zhang, J. H. *J. Mater. Chem.* **2011**, *21*, 16379.

(20) Liu, Y. F.; Zhang, X.; Hao, Z. D.; Wang, X. J.; Zhang, J. H. *Chem. Commun.* **2011**, *47*, 10677.

(21) Jia, Y. C.; Huang, Y. J.; Guo, N.; Qiao, H.; Zheng, Y. H.; Lv, W. Z.; Zhao, Q.; You, H. P. *J. Mater. Chem.* **2012**, *22*, 15146.

(22) Kim, J. S.; Kim, G. C.; Kim, T. W. *Appl. Phys. Lett.* **2004**, *85*, 3696.

(23) Rao, R. P. *J. Electrochem. Soc.* **2003**, *150*, H165.

(24) Huang, C. H.; Chen, T. M. *J. Phys. Chem. C* **2011**, *115* (5), 2349−2355.

(25) Li, G. G.; Geng, D. L.; Shang, M. M.; Zhang, Y.; Peng, C.; Cheng, Z. Y.; Lin, J. *J. Phys. Chem. C* **2011**, *115* (44), 21882.

(26) Li, G. G.; Zhang, Y.; Geng, D. L.; Shang, M. M.; Peng, C.; Cheng, Z. Y.; Lin, J. *ACS Appl. Mater. Interfaces* **2012**, *4* (1), 296.

(27) Geng, D. L.; Li, G. G.; Shang, M. M.; Yang, D. M.; Zhang, Y. Z.; Cheng, Y.; Lin, J. *J. Mater. Chem.* **2012**, *22*, 14262.

(28) Lü, W.; Hao, Z. D.; Zhang, X.; Luo, Y. S.; Wang, X. J.; Zhang, J. H. *Inorg. Chem.* **2011**, *50*, 7846.

(29) Larson, A. C.; Von Dreele, R. B. *Los Alamos Natl. Lab. [Rep.] LAUR* **1994**, *86*, 748.

(30) Ohashi, H.; Ii, N. *J. Jpn. Assoc. Mineral., Petrol. Econ. Geol.* **1978**, *73*, 267.

(31) Shannon, R. D. *Acta Crystallogr.* **1976**, *A32*, 751.

(32) Inokuti, M.; Hirayama, F. *J. Chem. Phys.* **1978**, *43*, 1965.

(33) Blasse, G. *Philips Res. Rep.* **1969**, *24*, 131.

(34) Verstegen, J. M. P. J. J.; Sommerdijk, L.; Verriet, J. G. *J. Lumin.* **1973**, *6*, 425.